Quantum Nano-Electronics

Hervé Courtois

Institut Néel
CNRS, Université Joseph Fourier and Grenoble INP

http://neel.cnrs.fr/spip.php?article804&lang=en
herve.courtois@neel.cnrs.fr

Part 4:
Mesoscopic superconductivity

Chapter 1:
General concepts

1.1 Andreev reflection

The Andreev reflection

At low energy, below the gap, no electron state in S.

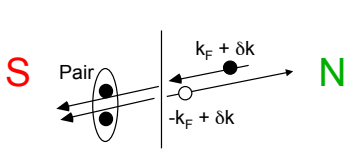

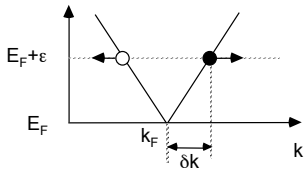

An incident electron is retro-reflected as a hole of opposite spin.
Electron and reflected hole have a wave-vector mismatch: $\delta k = k_F \frac{\varepsilon}{E_F}$

A Cooper pair (two electrons of opposite spin) is transmitted.

NOT an electron-hole pair in N because e- is present before, h after.
Two electron states occupation correlated: an Andreev pair.

1.2 BTK model

The Andreev reflection

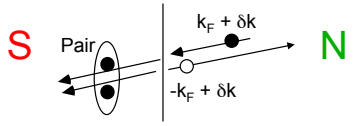

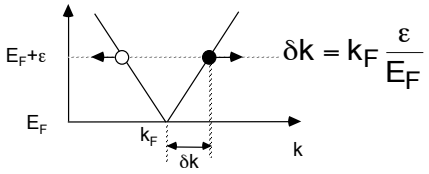

After diffusion over L, e and h are phase-shifted: $\delta\varphi = \delta k.x \approx \pi \frac{\varepsilon}{E_{Th}} = \pi \frac{L}{L_\varepsilon}$
x being the trajectory length = $v_F.L^2/D$.

Phase difference is small:
At a given position L, if energy ε is such that $\varepsilon < E_{th}$, $E_{Th} = \frac{\hbar D}{L^2} = \frac{\hbar}{\tau_D}$
E_{th} being the Thouless energy.

At a given energy energy ε, if distance is less than L_ε, $L_\varepsilon = \sqrt{\frac{\hbar D}{\varepsilon}}$
which the energy-dependent coherent length.

BTK model

Different possible process at a N-S interface:
incident particle 0,
Andreev reflection A,
specular reflection B,
transmission C, D.
A(E)+B(E)+C(E)+D(E)=1

Hypothesis of ballistic system.

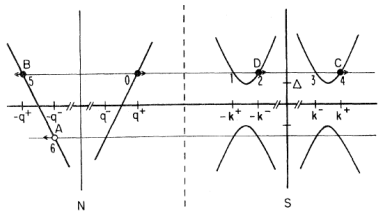

FIG. 4. Schematic diagram of energy vs momentum at *N-S* interface. The open circles denote holes, the closed circles electrons, and the arrows point in the direction of the group velocity. This figure describes an incident electron at (0), along with the resulting transmitted (2,4) and reflected (5,6) particles.

Transmission in the normal state parametrized with the interface parameter Z:

$$T = \frac{1}{1+Z^2}$$

Z = 0 corresponds to a transparent interface, large Z to the tunnel regime.

BTK model

Probability for every process can be calculated based on Bogoliubov-de Gennes equations + continuity equations.

Probabilities depend on bias.

Z = 0: A = 1 below the gap, C = 1 well above.

Large Z: B = 1 below, mix of B and C above.

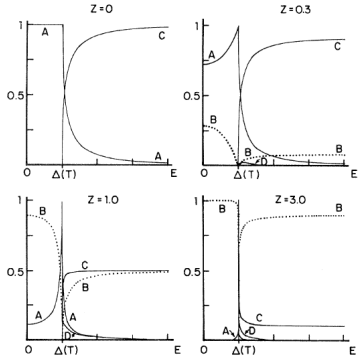

FIG. 5. Plots of transmission and reflection coefficients at *N-S* interface. *A* gives probability of Andreev reflection, *B* gives probability of ordinary reflection, *C* gives transmission probability without branch crossing, and *D* gives probability of transmission with branch crossing. The parameter *Z* measures the barrier strength at the interface.

BTK model

I-V are directly related to coefficient transmissions.

$$I = N(E_F) e v_F \int_{-\infty}^{+\infty} \left[1 + A(E) - B(E)\right]\left\{f(E - eV) - f(E)\right\} dE$$

Andreev reflection carries two charges instead of one:
Conductance doubled for Z = 0 below the gap.

For large Z:
one recovers the image of the S LDOS.
Smearing related to Z, not to temperature.

Here only the barrier conductance is considered.

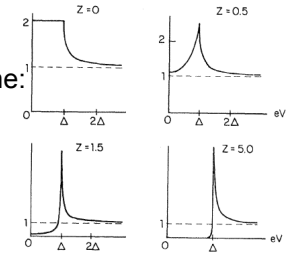

FIG. 7. Differential conductance vs voltage for various barrier strengths Z at $T=0$. This quantity is proportional to the transmission coefficient for electric current for particles at $E=eV$.

Andreev reflection vs spin-polarization

Polarization in a ferromagnet is defined: $P = \dfrac{N_\uparrow - N_\downarrow}{N_\uparrow + N_\downarrow}$

The conductance of a FN contact is:

$$G_{FN} = \frac{e^2}{h}\left(N_\uparrow + N_\downarrow\right)$$

The majority spin has a probability $\dfrac{N_\downarrow}{N_\uparrow}$ to be transmitted.

$$G_{FS} = \frac{e^2}{h}\left(2N_\downarrow + 2\frac{N_\downarrow}{N_\uparrow}N_\uparrow\right) = 4\frac{e^2}{h}N_\downarrow = 2G_{FN}\left(1-P\right)$$

The differential conductance at zero bias gives access to the spin polarisation. If P > ½, then $G_{FS} < G_{FN}$

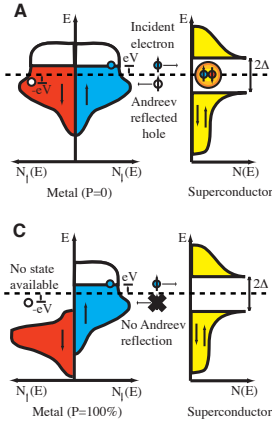

Measuring spin polarization

Point contact Andreev Reflection (PCAR): a wire of a given material pressed against a superconducting film.

Depending on the material, the conductance ratio varies from about 2 to almost zero.

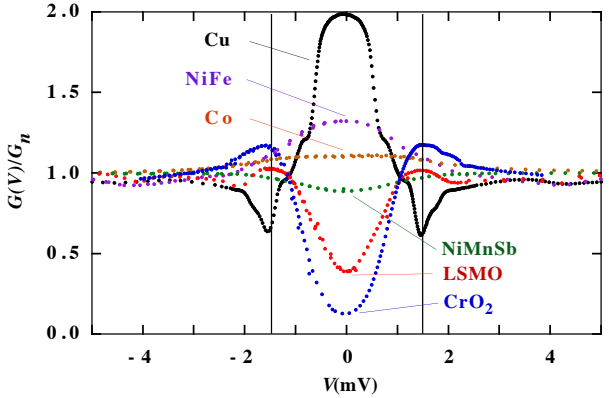

R. J. Soulen et al, Science 282, 85 (1998).

Chapter 2:
Superconducting proximity effect

Usadel equations

Andreev pairs induced in the normal metal create superconducting-like properties.
The elastic mean free path is shorter than every other characteristic length.
A diffusion eq. describes the spatial dependence of the Andreev pairs density.

$$\frac{\hbar D}{2}\partial_r^2\theta + \left(2i\varepsilon - \left[\partial_r\chi - 2eA\right]^2\cos\theta - \frac{\hbar}{\tau_\varphi}\cos\theta\right)\sin\theta = 0$$

Complex proximity angle: $\theta(x,\varepsilon) = \theta_1 + i\theta_2$

With no phase gradient and zero magnetic field:

$$\hbar D\partial_x^2\theta + \left(2i\varepsilon - \frac{\hbar}{\tau_\varphi}\cos\theta\right)\sin\theta = 0$$

A. Golubov et al., J. of Low Temp. Phys. 61, 83 (1998); W. Belzig et al., Phys. Rev. B 54, 9443 (1996)

2.1 Usadel equations

Usadel equations

Usadel equations gives access to every physical quantity.

Pair amplitude: $F(\varepsilon,x) = -i\sin\theta$

Local Density Of States: $\nu(\varepsilon,x) = \nu_0\cos\theta_1\cosh\theta_2$

Local conductivity enhancement: $\sigma(\varepsilon,x) = \sigma_N\cosh^2\theta_2$

Boundary conditions:

at infinity in N: $\theta_N = 0$

at infinity in S: $\theta_S = \frac{\pi}{2} + \operatorname{arg\,th}\left(\frac{\varepsilon}{\Delta}\right)$ gives the BCS DOS.

Usadel equations: a simple case

Consider a simple N-S junction,
No inverse proximity effect: $\theta_S = \frac{\pi}{2} + \arg\text{th}\left(\frac{\varepsilon}{\Delta}\right)$ verified at the interface x = 0.

Linear approximation: $\sin\theta \approx \theta$

Simplified eq.: $\hbar D\partial_x^2\theta + \left(2i\varepsilon - \frac{\hbar}{\tau_\varphi}\right)\theta = 0$

In this case this same equation holds for the pair amplitude F.

Boundary condition at low energy: $\theta(x=0) = \frac{\pi}{2}$

Solution in the regime $\tau_\varphi \to \infty$: $\theta(\varepsilon, x) = \frac{\pi}{2}\exp\left[(i-1)\frac{x}{L_\varepsilon}\right]$

Decay lengh given by L_ε.
In the general case, a finite τ_φ adds an exponential cut-off at a distance L_φ.

2.2 The spectral conductance and the re-entrance effect

The N-S junction

Solution in the regime $\tau_\varphi \to \infty$: $\theta(\varepsilon, x) = \frac{\pi}{2}\exp\left[(i-1)\frac{x}{L_\varepsilon}\right]$

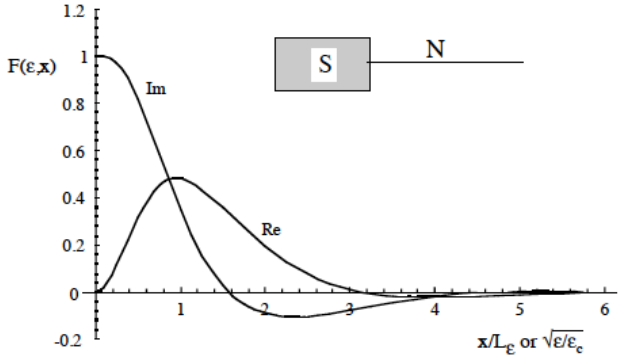

Fig. 2. Plot of the imaginary and real part of the pair amplitude wave-function $F(\epsilon, x)$ calculated in the framework of the linearized Usadel equation. The horizontal axis can be read either as the distance x normalized to the energy-dependent coherence length L_ϵ (here the energy ϵ is fixed) or as the square root of the energy ϵ in units of the local energy scale $\epsilon_x = \hbar D/x^2$ related to the distance x (here the distance x is fixed). Inset : the considered sample geometry made of an unfinite N wire in contact with a superconductor S.

The spectral conductance

The proximity effect modifies the conductance.
One can view the effect as a local conductivity enhancement.

$$\sigma(\varepsilon, x) = \sigma_N \cosh^2\theta_2 = \sigma_N \cosh^2\left(\frac{\pi}{2}\exp\left[-\frac{x}{L_\varepsilon}\right]\sin\frac{x}{L_\varepsilon}\right)$$

Spectral conductance: depends on electron energy.

Spectral conductance: $g(\varepsilon) = S\left[\int_0^L \frac{1}{\sigma(\varepsilon, x)}dx\right]^{-1}$

As θ_2 is non-monotonous, $g(\varepsilon)$ has a maximum as a function of energy.
Location determined by the Thouless energy.

The spectral conductance

Spectral conductance can be measured as the zero-temperature differential conductance:

$$\frac{dI}{dV}(V=\varepsilon/e, T=0) = g(\varepsilon)$$

The zero-bias conductance varies with temperature:

$$G(V=0,T) = \frac{dI}{dV}(V=0,T) = \int_{-\infty}^{+\infty} g(\varepsilon) \frac{1}{4k_B T \cosh^2(\varepsilon/2k_B T)} d\varepsilon$$

$$\frac{df}{dE}$$

Re-entrance effect

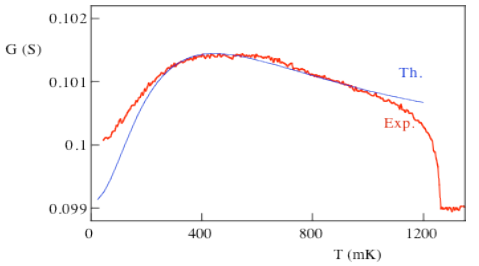

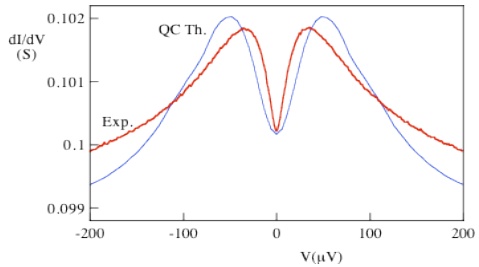

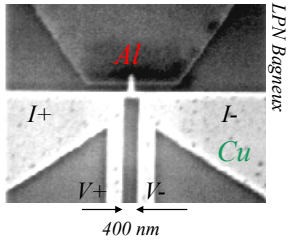

Conductance maximum at eV, $k_B T \approx E_{Th}$ = 12 μV, 140 mK

P. Charlat, H. Courtois, P. Gandit, A. Volkov, D. Mailly and B. Pannetier, Phys. Rev. Lett. 77, 4950 (1996)

2.3 Long-range coherence of Andreev pairs

Long range coherence of Andreev pairs

Consider Usadel equation at zero energy:

$$\hbar D \partial_x^2 \theta + \left(2i\varepsilon - \frac{\hbar}{\tau_\varphi}\right)\theta = 0 \quad \Rightarrow \quad \hbar D \partial_x^2 \theta = \frac{\hbar}{\tau_\varphi}\theta$$

Decay of Andreev pairs density only on a length scale L_φ.

At a distance L, Andreev pairs with an energy below the Thouless energy E_{Th} remain coherent.

To be compared with the energy distribution width $k_B T$ of electrons participating to transport.

The fraction of coherent Andreev pairs is then $\frac{E_{Th}}{k_B T}$

Long range coherence of Andreev pairs

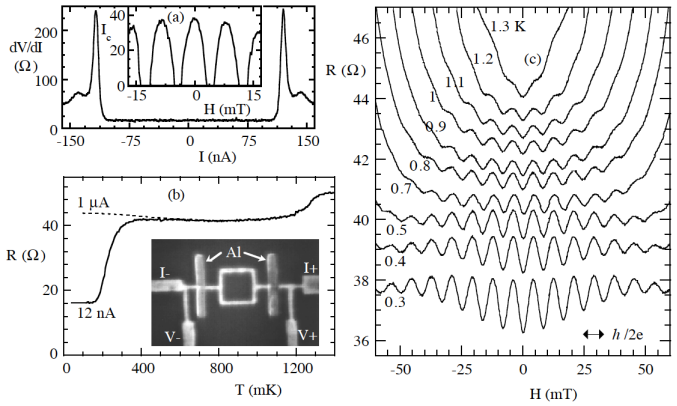

Fig. 4. (a) Sample differential resistance dependence on the bias current at 40 mK. Inset shows the critical current (in nA) measured at 150 mK with a 25Ω differential resistance criteria as a function of the magnetic field. Flux periodicity of the critical current oscillations is $h/2e$. (b) Temperature dependence of the sample resistance with a measurement current 12 nA and 1 μA. Inset : Micrograph of a typical sample made of a Cu square loop with 4-wire measurement contacts, in contact with two Al islands (vertical). Size of the loop is 500 X 500 nm^2, width 50 nm, thickness 25 nm. Centre-to-centre distance between the 150 nm wide Al islands is 1 μm. The length L of the N part of the S-N-S junction is 1.35 μm. The elastic mean free path is 16 nm, the thermal coherence length is 99 nm at 1 K and the phase-breaking length is about 1.9 μm. (c) : Low-field magnetoresistance for T = 0.3; 0.4; 0.5; 0.7; 0.8; 0.9; 1; 1.1; 1.2 and 1.3 K. Curves have been arbitrarily shifted for clarity. Oscillations of periodicity $h/2e$ and amplitude e^2/h at T = 0.8 K are visible.

Long range coherence of Andreev pairs

Magnetoresistance oscillations amplitude decay as 1/T !

Proof for long-range coherence of Andreev pairs.

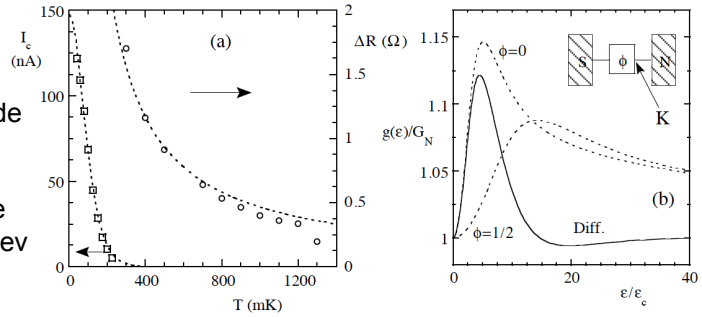

Fig. 5. (a) Left scale : Temperature dependence of the critical current derived from Fig. 4 data with a 25Ω differential resistance criteria. Dashed line is a guide to the eye. Right scale : Temperature dependence of the amplitude of the magnetoresistance oscillations, Dashed line is a 1/T power-law fit. (b) Sketch of the spectral conductance as a function of the voltage bias in a loop-shaped sample with zero flux and half a flux quantum in the loop (dotted lines). The ratio distance S-K over distance S-N is 0.6. The full curve gives the difference of spectral conductance between these two cases. Inset shows the sample model. The arrow shows the point K where the pair amplitude is zero when the flux through the loop is $\varphi = \phi_0/2$.

H. Courtois et al, Phys. Rev. Lett. 76(1), 130 (1996).

2.4 The LDOS

Samples for LDOS measurement

Geometry :

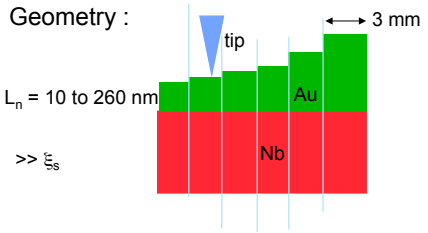

From transport measurements :

$l_{e,s}$ = 5.4 nm $\quad \xi_s = \sqrt{\frac{\hbar D_s}{2\Delta}} = 23.2\text{nm}$

$l_{e,n}$ = 36.1 nm $\quad \xi_n = \sqrt{\frac{\hbar D_n}{2\Delta}} = 60.8\text{nm}$

100 mK STM image

(L_n = 72 nm sample)

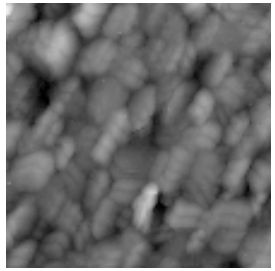

410 x 410 nm²

R_t = 10 MΩ

rms roughness 3.4 nm

The proximity LDOS

Mini-gap scales with the Thouless energy.

Structure (max or min) at Δ for every L_n

Non-zero LDOS at the Fermi level for large L_n (not a ballistic effect) + Subgap structures

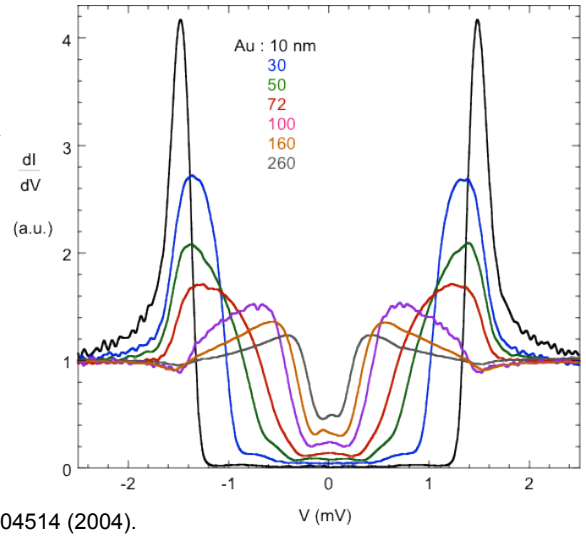

A. K. Gupta et al, Phys. Rev. B, 69, 104514 (2004).

Chapter 3:
Electronic thermometry and cooling

3.1 Electronic thermometry

Charge current in a N-I-S tunnel junction

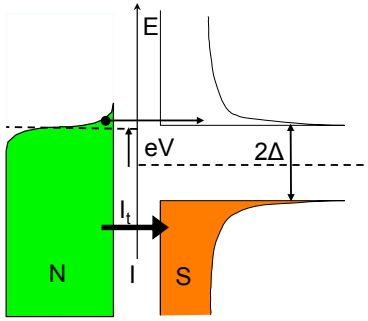

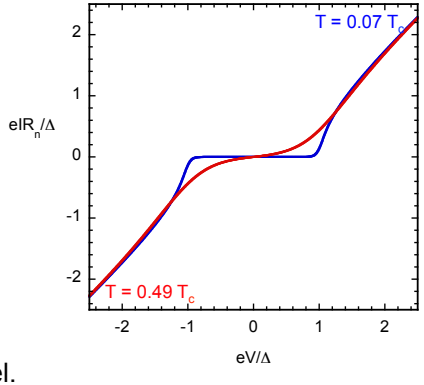

Only electrons above the gap can tunnel.

IV step rounded by temperature.

$$I_T = \frac{1}{eR_n}\int_{-\infty}^{+\infty} N_S(E)\left[f_S(E-eV) - f_N(E)\right]dE$$

Charge current in a N-I-S tunnel junction

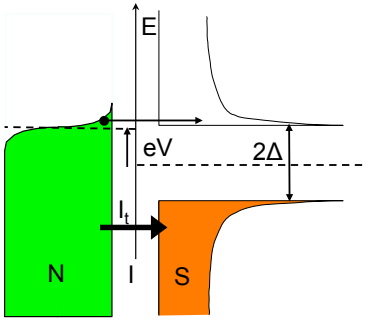

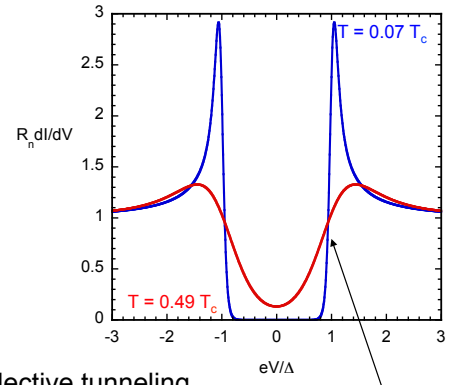

slope α T in log scale

The energy gap induces an energy-selective tunneling.

Charge current (antisymmetric in bias):

$$I_T = \frac{1}{eR_n}\int_{-\infty}^{+\infty} N_S(E)\left[f_S(E-eV) - f_N(E)\right]dE$$

A N-I-S junction as a thermometer (1)

$$I = \frac{1}{eR_N}\int_{-\infty}^{+\infty} N_S(E)\left[f_N(E-eV) - f_S(E)\right]dE$$

DOS

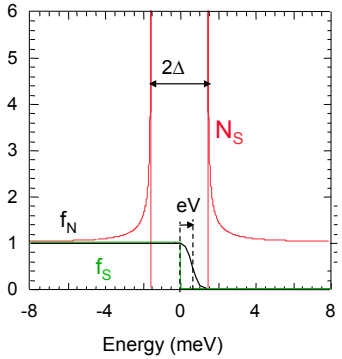

Consider T_S small, T_N to be measured,

$eV < \Delta \approx E$

$$f_N(E-eV) - f_S(E) \approx \exp\left(-\frac{E-eV}{k_B T}\right)$$

Sub-gap current:

$$eI = \frac{1}{R_N}\int_{-\infty}^{+\infty} N_S(E)\exp\left(-\frac{E-eV}{k_B T}\right)dE = eI_0 \exp\left(\frac{eV}{k_B T}\right)$$

A N-I-S junction as a thermometer (2)

$$I = I_0 \exp\left(\frac{eV}{k_B T}\right)$$

The sub-gap current depends strongly on V and T.

Usual mode: fixed bias current, voltage drop measured.

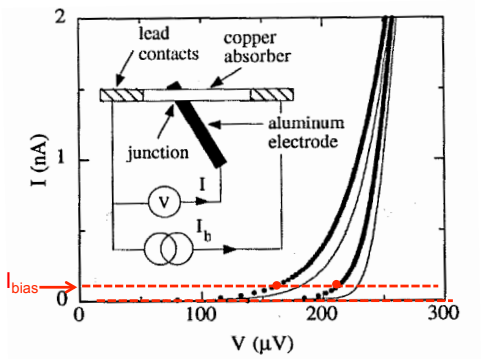

FIG. 1. Current-voltage characteristics of the SIN junction. The solid curves correspond to temperatures of 40 and 300 mK from right to left, with zero power dissipated in the absorber. The dotted curves correspond to a base temperature of 40 mK, but with 20 fW and 2 pW dissipated in the metal absorber, respectively. The inset is a schematic of the device. The power dissipated in the resistance R of the absorber is $I_b^2 R$.

M. Nahum and J. Martinis, Appl. Phys. Lett. 63, 3075 (1993).

Application of N-I-S junction thermometry

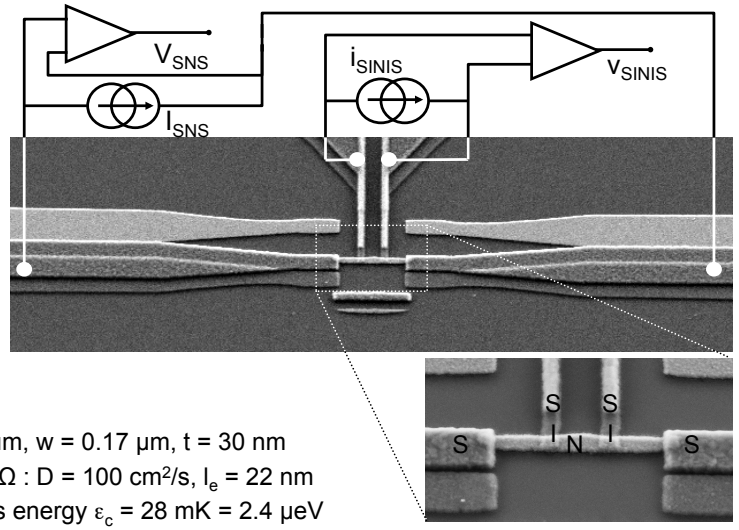

L = 1.5 μm, w = 0.17 μm, t = 30 nm

R_N = 10 Ω : D = 100 cm^2/s, l_e = 22 nm

Thouless energy ε_c = 28 mK = 2.4 μeV

0.5 μm

The SINIS thermometer calibration

I(V) of the double N-I-S junction at thermal equilibrium.

Calibration at a fixed current bias: no saturation down to 40 mK.

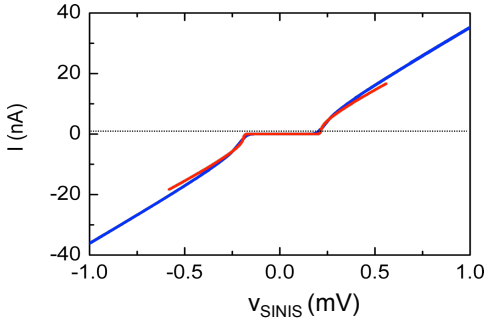

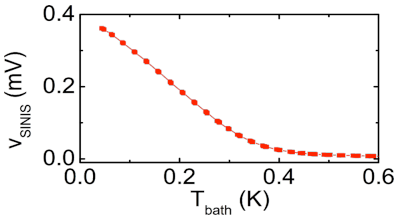

Hypothesis of quasi-equilibrium in the N metal: T_e can be defined.

I(V) and electron temperature

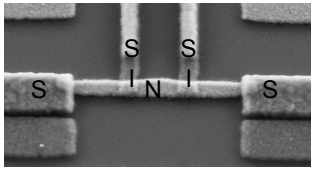

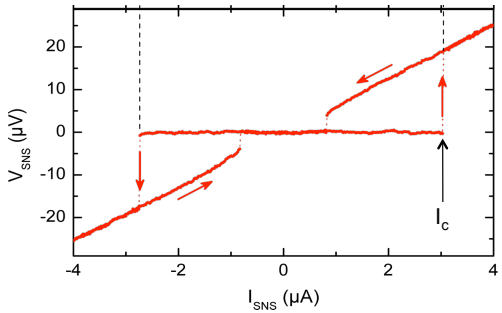

I(V) and electron temperature

The electron thermometer correlates to switching.

thermal origin of the hysteresis. T_e up to 0.6 K !

H. Courtois, M. Meschke, J. T. Peltonen, and J. P. Pekola, PRL 101, 067002 (2008).

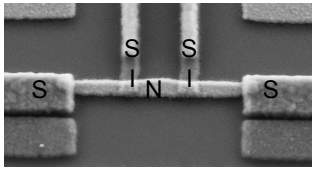

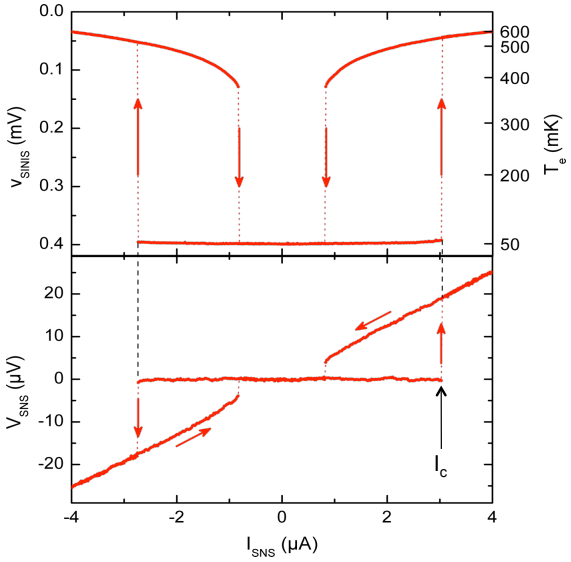

3.2: Electron cooling in a S-I-N-I-S junction

Charge current in a N-I-S tunnel junction

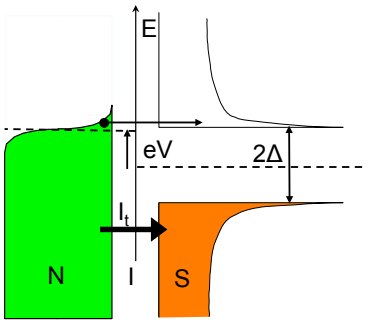

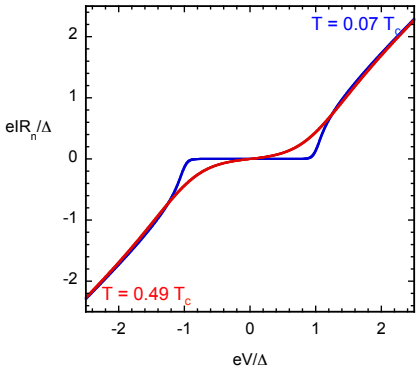

Only electrons above the gap can tunnel.

IV step rounded by temperature.

$$I_T = \frac{1}{eR_n}\int_{-\infty}^{+\infty} N_S(E)\left[f_S(E-eV) - f_N(E)\right]dE$$

Heat current in a N-I-S tunnel junction

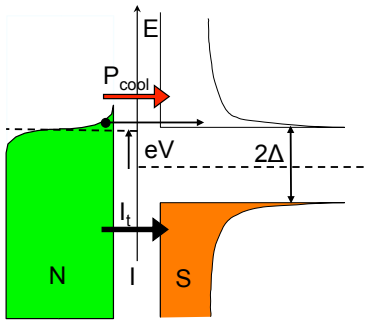

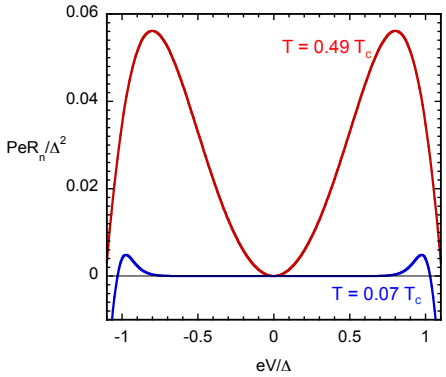

Heat current (symmetric in bias):

$$P_{cool}(V) = \frac{1}{e^2R_n}\int_{-\infty}^{+\infty}(E-eV)N_S(E)\left[f_N(E-eV) - f_S(E)\right]dE$$

$I_TV + P_{cool}$ is deposited in S.

Heat current in a N-I-S tunnel junction

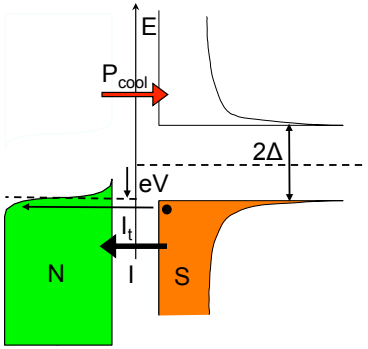

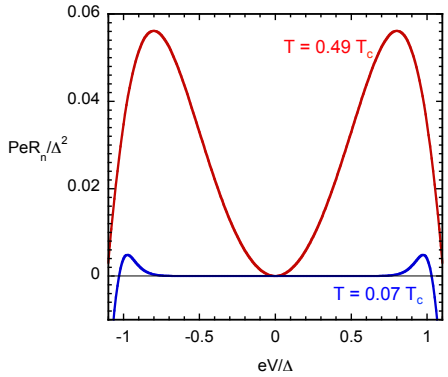

Heat current (symmetric in bias):

$$P_{cool}(V) = \frac{1}{e^2R_n}\int_{-\infty}^{+\infty}(E-eV)N_S(E)\left[f_N(E-eV) - f_S(E)\right]dE$$

$I_TV + P_{cool}$ is deposited in S.

Cooling power

Bias-dependent, optimum

$$P_{max} = \frac{\Delta^2}{e^2R_T}\left[0.59\left(\frac{k_BT_N}{\Delta}\right)^{3/2} - \sqrt{\frac{2\pi k_BT_S}{\Delta}}\exp\left(-\frac{\Delta}{k_BT_S}\right)\right]$$

$T_N << T_C$

reached at

$V \approx \Delta/e - k_BT$

Max cooling power at:

$T \approx T_C/3$

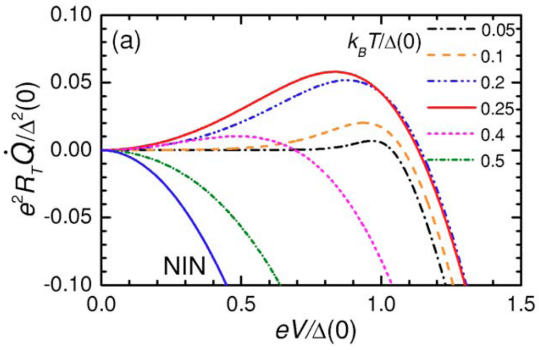

The S-I-N-I-S geometry

Two cooling junctions in series:
double cooling power + good thermal insulation of cooled metal.

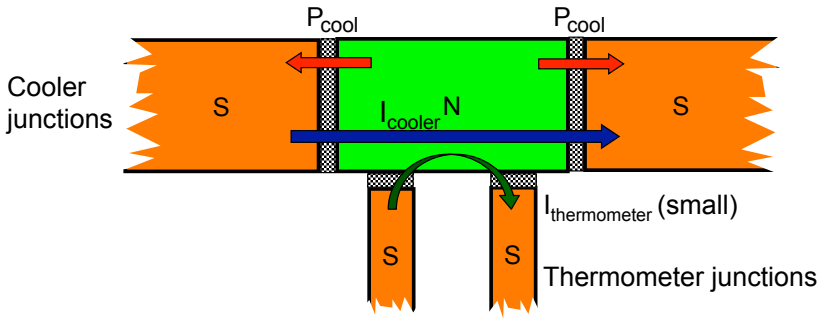

Plus two thermometer junctions for independent probing.

Electronic cooling and thermometry

Cooling from 300 mK down to 100 mK can be achieved in a S-I-N-I-S geometry.

Above the gap: qp injection and heating

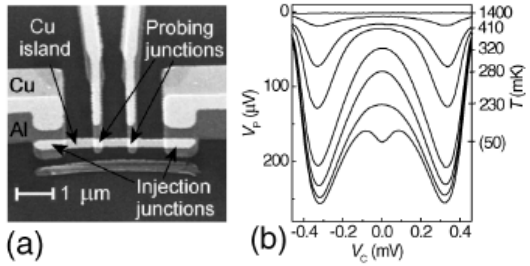

FIG. 1. Scanning electron micrograph of a typical cooler sample in (a), and cooling data in (b), where voltage V_P across the probe junctions in a constant current bias (28 pA) is shown against voltage V_C across the two injection junctions. Cryostat temperature, corresponding to the electron temperature on the N island at $V_C = 0$ is indicated on the right vertical axis. Below 100 mK this correspondence is uncertain, because of the lack of calibration and several competing effects to be discussed in the text.

J. Pekola, T.T. Heikkila, A. M. Savin, J.T. Flyktman, F. Giazotto, F.W.J. Hekking, Phys. Rev. Lett. 92, 056804 (2004): Helsinki.

The S-I-N-I-S samples

Probe: metal strongly thermalized, no cooling.

Cooler: weakly coupled to pads, strong cooling, R_t about 1 kΩ.

No electron thermometer.

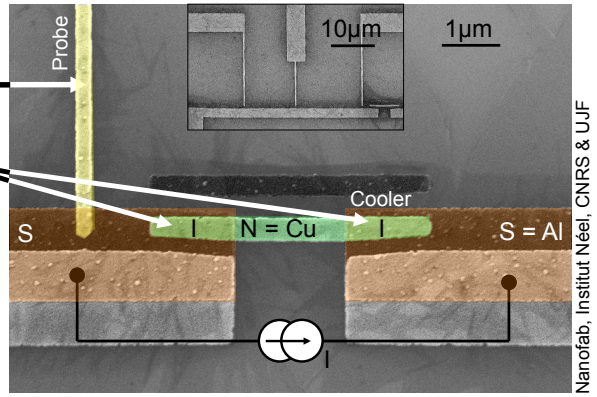

Al-AlO_x-Cu tunnel junctions: high stability and good reproducibility.

Al behaves as a perfect BCS superconductor.

The differential conductance

T_{base} = 320 mK

High resolution measurement (log scale)

Probe follows isothermal prediction at T_{base}.

$$el(V) = G_T \int_{-\infty}^{+\infty} N_S(E)\left[f_S(E) - f_N(E + eV)\right]dE$$

Cooler behaves differently

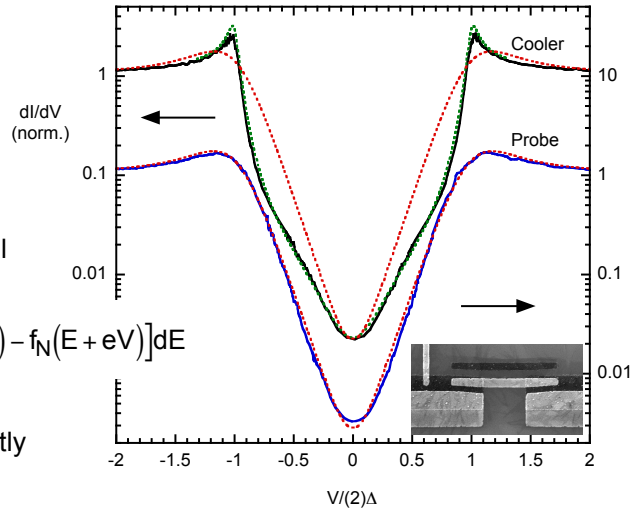

Extraction of the electron temperature

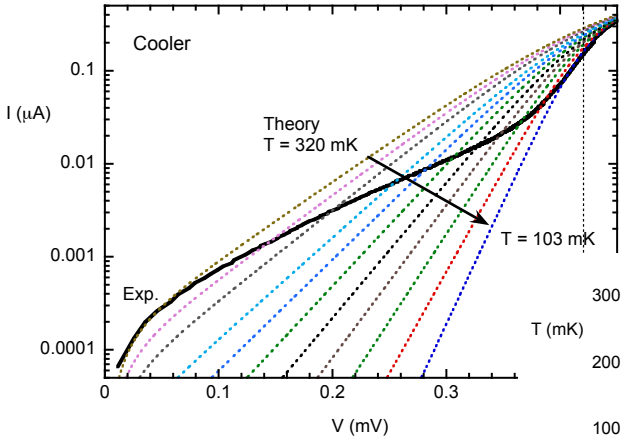

Inelastic scattering strong enough to define an electron temperature.

Superposition of exp. data with theoretical I-V

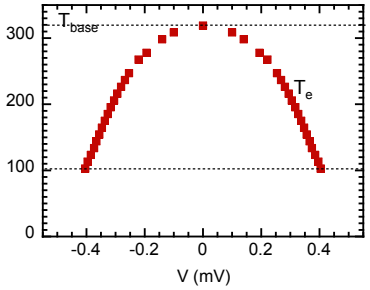

Determination of the bias-dependent electron temperature

The thermal model

Power flow from N electrons to the S electrodes remaining at bath temperature

$$P_{cool}(V) = \frac{1}{eR_n}\int_{-\infty}^{+\infty}(E - eV)N_S(E)\left[f_S(E) - f_N(E + eV)\right]dE$$

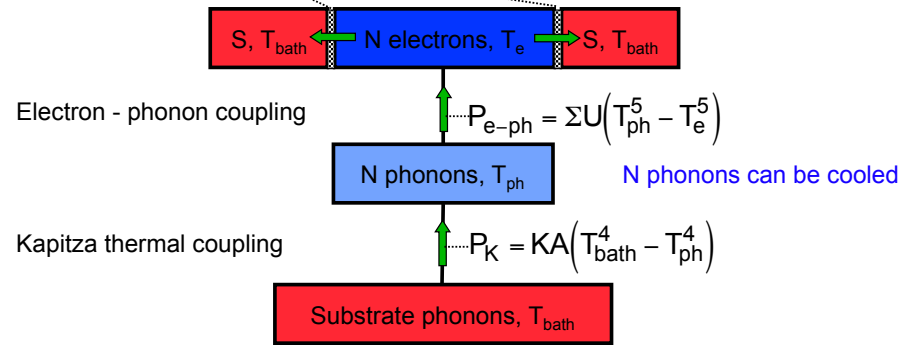

The phonon temperature

Two free fit parameters:

Σ = 2 nW.μm^{-3}.K^{-5}

KA = 66 pW.K^{-4}

Determination of both electron (T_e) and phonon (T_{ph}) temperature.

Phonons cool down by about 50 mK.

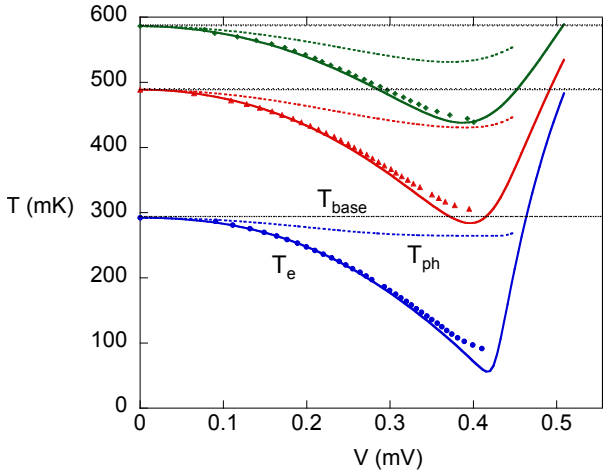

S. Rajauria, P. S. Luo, T. Fournier, F. W. J. Hekking, H. Courtois, and B. Pannetier, Phys. Rev. Lett. 99, 047004 (2007).

Applications

A NTD bolometer is cooled from 320 mK down to 225 mK.

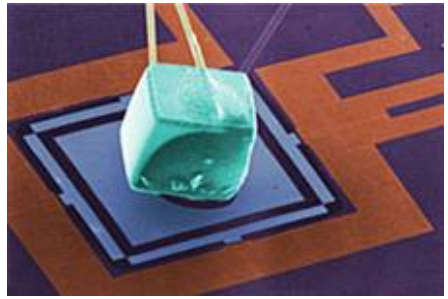

FIG. 2. Scanning electron microscope image of NIS refrigerator with attached neutron transmutation doped (NTD) germanium resistance thermometer. One of the four pairs of refrigerator junctions is circled. Additional junctions for thermometry are located beneath the NTD. The ratio of the volumes of the NTD and the refrigerating junctions is comparable to the ratio of the volumes of the Statue of Liberty and an ordinary person (about 11 000).

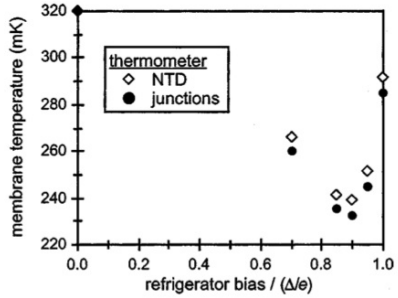

FIG. 3. Measured membrane temperature plotted vs refrigerator bias. Temperature measurements are shown for the NTD thermometer and a junction pair underneath the NTD. The peak cooling of the NTD corresponds to a tripling of its physical resistance. The peak cooling occurs for refrigerator bias values near $0.9\Delta/e$, as expected.

Cooling efficiency

Dissipated power (by the bias source) in the superconductor : I.V

Cooling power in the normal metal : $P_{cool} \approx I(\Delta - eV)$

At the optimum bias, thermal qp overcome the gap : $\Delta - eV \approx k_B T_e$

Efficiency $\eta = \frac{P_{cool}}{I.V} \approx \frac{\Delta - eV}{\Delta} \approx \frac{T_e}{\Delta}$

$\Delta = 1.76\ k_B\ T_c$; $T_c = 1.3$ K; $T_e = 0.1$ K ⟹ $\eta = 4$ %

Rather low efficiency at low temperature,
Energy dissipation in the superconductor is a major issue.